

Spatial correlation of self-assembled isotopically pure Ge/Si(001) nanoislands

Satoru Miyamoto,^{1,*} Oussama Moutanabbir,^{1,2,†} Eugene E. Haller,³ and Kohei M. Itoh^{1,‡}

¹*School of Fundamental Science and Technology, Keio University, 3-14-1 Hiyoshi, Yokohama 223-8522, Japan*

²*Max Planck Institute of Microstructure Physics, Weinberg 2, Halle (Saale) D-06120, Germany*

³*University of California at Berkeley and Lawrence Berkeley National Laboratory, Berkeley, California 94720, USA*

(Received 24 December 2008; revised manuscript received 11 February 2009; published 9 April 2009)

By using a statistical method based on Voronoi tessellation, we investigated the nucleation of strain-driven self-assembled Ge/Si(001) nanoislands and their dynamic interaction with the local environment. The evolution of the composition and strain during the growth process was also studied by Raman scattering. The use of isotopically purified ⁷⁶Ge source allows the observation of faint features in the three-dimensional nanoisland Raman signal at the early stage of the growth. The nucleus critical sizes are deduced from the scaling behavior of the Voronoi cell areas and the grown island volumes. The relatively small critical size suggests a stabilizing role of Si atoms and surface imperfections. Additionally, we found that the nucleation process on the metastable two-dimensional layer cannot only be described by the capture of newly deposited Ge atoms, but it is strongly governed by the diffusive interaction with the SiGe alloyed layer.

DOI: [10.1103/PhysRevB.79.165415](https://doi.org/10.1103/PhysRevB.79.165415)

PACS number(s): 68.55.A–, 68.43.Jk, 81.07.Ta, 28.60.+s

I. INTRODUCTION

Strain-mediated self-assembly is a versatile process by which a variety of quantum and nanoscale structures can be obtained providing a wide spectrum of potential applications in nanoelectronics, optoelectronics, and quantum information.¹ In the case of small lattice mismatched heteroepitaxy, the formation of nanostructures is governed by the Stranski-Krastanow (SK) growth mode.² This growth mode is characterized by the transition from two-dimensional (2D) layer-by-layer growth to three-dimensional (3D) islanding which occurs beyond a critical thickness of a few atomic layers to relieve the compressive strain. At the atomic scale, the nucleation process is triggered by the interaction of deposited adatom with other adatoms or surface defects resulting in stable nuclei. These nuclei grow to mature 3D islands by capturing more atoms. The quantitative description of the atomic transport during the nucleation and growth remains a formidable challenge. For its simplicity, Ge deposition on Si has attracted a great deal of attention as a model system to explore the subtle details in SK growth and to investigate the underlying physics of strain-driven nucleation. At relatively low temperatures ($T < 600$ °C), only hut clusters bounded by {105} facets are formed due to the kinetic restrictions.³ In contrast, coherent islands with steeper well-defined facets such as square-based pyramids or round-based domes are formed at temperatures above 600 °C.⁴ Si-Ge intermixing in self-assembled nanostructure leads to the smearing out of the atomlike potential well expected for a pure Ge quantum dot.⁵ This phenomenon is unavoidable and occurs at the early stage of the Ge deposition on the Si substrate.^{6,7}

In this paper, the nucleation and growth of 3D islands on the alloyed 2D layer are investigated at the growth temperature $T = 620$ °C. At this temperature, both kinetics and thermodynamics play competitive roles. In our study, we combine the geometrical assessment with the composition and strain characterization to trace the nucleation and growth processes from the nuclei to the 3D islands. Beyond the critical thickness, the nuclei greater than a critical size are gen-

erated on the 2D layer. The nucleation process increases the fraction of the surface area covered with the diffusion cells corresponding to circles with a radius equal the diffusion length centered on the nucleus. The adatoms within the diffusion cells contribute to the growth of the existing stable nuclei and those outside aggregate, leading to the generation of nuclei. When the entire surface is fully covered by ensembles of diffusion cells, most of the adatoms can steadily participate in the growth of the islands. The capture zone model is introduced to describe the competition among the coexisting islands to capture the deposited adatoms. This simple model can be investigated with the help of the Voronoi cell (Wigner-Seitz cell), which is defined as the region enclosed by the perpendicular bisectors between the centers of the nearest neighboring islands.^{8–10} The intersection between the Voronoi cell and the diffusion cell gives the capture zone associated with each island. This allows us to analyze the tendency of adatoms to be incorporated into the closest island. Based on this geometrical correlation between the Voronoi cells and the resulting 3D islands, we show that the growth of 3D islands involves not only Ge atoms evaporated on the wetting layer but also Si and Ge atoms transported from the SiGe alloy wetting layer, the underlying substrate, and probably the neighboring strained islands. The scaling analyses of the grown island volumes and the Voronoi cell areas experimentally determine the critical size of nuclei leading to pyramids and domes. In addition, our analysis contributes to elucidate the evolution of the 3D islands in their coexisting states. Each nucleus grows rather independently from others, eroding the intermixed wetting layer surrounding them. When the distance to the nearest neighbor becomes significantly small, the smaller pyramids act as precursors for material redistribution toward the adjacent larger domes. Such strong material-mediated interactions among the intermixed wetting layer and the neighboring islands of different sizes were reported previously based on the experimental observation of wetting layer consumption^{11–13} and anomalous coarsening.^{14,15} However, the composition within the grown islands and the role of strain on the intrasland interaction are still debated.^{16–19}

Therefore, we employ Raman scattering spectroscopy to provide a comprehensive and quantitative overview of the mass interactions during nucleation and growth of 3D islands.

II. EXPERIMENTAL DETAILS

The Ge island growth was performed on a *p*-type Si(001) substrate using solid source molecular-beam epitaxy (MBE). Before being introduced into the chamber, the substrate was chemically cleaned by the Ishizaka-Shiraki method.²⁰ The protective oxide film was removed in the growth chamber by annealing the substrate at 800 °C. The surface cleanliness, especially *regarding carbon*, was confirmed by the (2×1) streaky pattern of reflection high-energy electron diffraction. After the cleaning process the temperature was gradually reduced to $T=620$ °C for Ge deposition. Ge was deposited onto the substrate from an isotopically purified ⁷⁶Ge solid source heated at 1160 °C in an effusion cell. The pressure in the chamber during the growth was kept in the range of 10^{-10} Torr. Here the deposition rate of ⁷⁶Ge was fixed at 0.04 ML/s (1.0 ML= 6.78×10^{14} atoms/cm²). The growth rate was determined using Rutherford backscattering spectrometry. The substrate was cooled down to room temperature immediately after the growth. The surface morphology was investigated by *ex situ* atomic force microscope (AFM) in tapping mode. The critical thickness of 2D-3D transition was defined as the maximum Ge coverage at which no 3D islands were observed by AFM. Under our growth conditions, this thickness is found to be $WL=4.4 \pm 0.1$ ML. The aim of the present work is the investigation of the nucleation and growth of self-assembled Ge islands on the 2D layer. Therefore, the “zeroth monolayer,” the starting point, is defined as the point at which the wetting layer is completed. This means, for example, that 1.0 ML growth from now on refers to the growth of a 4.4 ML wetting layer followed by a 1.0 ML deposition that induces the 3D islanding via the SK mode. Micro-Raman scattering spectroscopy was carried out at room temperature using Ar⁺ 514.5 nm laser focused to a 1- μ m-diameter spot. The backscattered light was dispersed by a single spectrometer and detected by a charge coupled device. The spectral distance between adjacent channels is 0.7 cm⁻¹.

III. RESULTS AND DISCUSSIONS

The correlation between the volume of the grown 3D island and the corresponding Voronoi cell areas is an important index to reveal the dynamic behaviors of adatoms on the 2D layer. If the correlation coefficient is close to unity, the capture zone model would turn out to be valid, indicating that the adatoms on the surface would tend to be incorporated into the nearest neighboring islands.⁹ Figure 1 shows the distribution of the volume of the 3D islands as a function of the corresponding Voronoi cell areas by evaluation of 500 islands at given amount of Ge deposited on the 2D layer. Clearly, the 3D islands are separated into two groups, small pyramids and relatively large domes, by the boundary set at the critical volume of $V_c=1.2 \times 10^4$ nm³. The insets display AFM images of samples obtained upon deposition of 0.2,

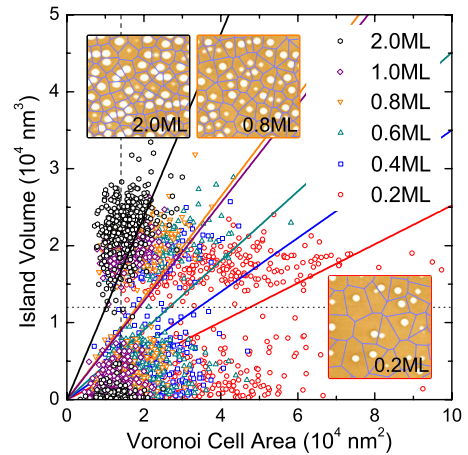


FIG. 1. (Color online) Distributions of the island volumes as a function of the corresponding Voronoi cell areas at 0.2, 0.4, 0.6, 0.8, 1.0, and 2.0 ML. The insets display AFM images (1×1 μm^2) for the Ge deposition of 0.2, 0.8, and 2.0 ML. The network superimposed on AFM images shows the Voronoi tessellation calculated from the center of each island. The horizontal dotted line shows the critical volume of $V_c=1.2 \times 10^4$ nm³ separating between small pyramids and large domes. The solid lines are the best linear fits to obtain the correlation coefficients. The vertical broken line denotes the average Voronoi cell area at the steady-state regime.

0.8, and 2.0 ML. The network superimposed on AFM images shows the Voronoi tessellation calculated from the center of each island. The validity of the capture zone model in the deposition range of 0.2–4.0 ML is statistically analyzed by the correlation coefficient r [Fig. 2(a)]. The evolution of the island density is also an important parameter projecting the nucleation frequency [Fig. 2(b)]. By assuming the validity of the capture zone model, the nucleation process can be described as follows:²¹ initially the number of nuclei is so small that the wetting layer surface cannot be covered completely with the diffusion cells. This manifests as a poor correlation because of the break of the Voronoi cell approximation for the capture zone. Then the adatoms within the diffusion cells can be gathered into the stable nuclei whereas the continuous nucleation outside promotes the branching of the Voronoi boundaries. The correlation coefficient is improved due to the exclusive generation of nuclei until 3D island density stops increasing. When the diffusion cells overlap with each other, most of adatoms can contribute to the growth of 3D islands instead of nucleation at the steady-state regime. Beyond 1.0 ML, the Voronoi cell areas converge at the vertical broken line in Fig. 1. At this regime, the correlation coefficient should approach unity as the Voronoi cells would coincide with the diffusion cells. However, it takes a value far below unity, as shown in Fig. 2(a), implying that the growth of 3D islands involves more complex processes than this simple model that considers the deposited Ge adatoms as the unique source of material. More specifically, the intermixed wetting layer and the underlying substrate in the vicinity of islands must be taken into account as material resources. It is worth pointing out that trenches form around the islands indicating the transfer of the material to the growing islands.²² As it is demonstrated below, this additional source of atoms

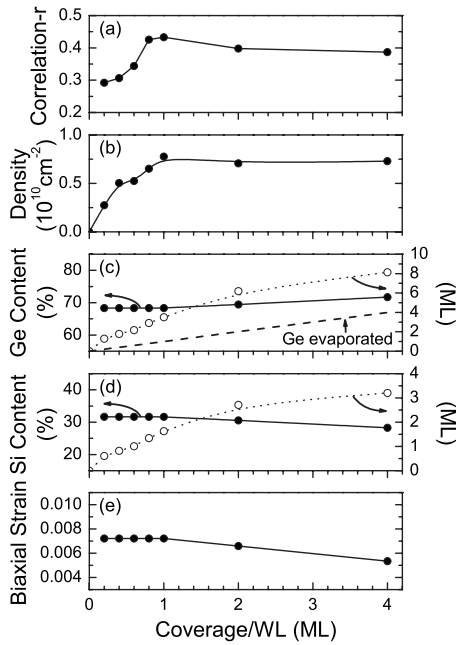


FIG. 2. Evolution as a function of the coverage of: (a) the correlation coefficient r ; (b) the island density; (c) the Ge content; (d) the Si content; and (e) the compressive biaxial strain (solid circles). Open circles in (c) and (d) show the total amounts of Ge and Si atoms in 3D islands calculated from the effective thickness on the wetting layer. The broken line in (c) shows the amount of deposited Ge atoms.

plays an important role in the nucleation process.

In order to further understand the nucleation process, we evaluated the scaling behavior of the Voronoi cell areas and the grown 3D island volumes. The scaling function for the distribution of the Voronoi cell areas is described by the semiempirical gamma distribution (SGD),⁸

$$\Pi_{\alpha}(x) = \frac{\alpha^{\alpha}}{\Gamma(\alpha)} x^{\alpha-1} \exp(-\alpha x), \quad (1)$$

where $\Gamma(\alpha)$ is Euler's gamma function and x is the Voronoi cell area scaled with its average value. The coefficient α denotes the degree of spatial correlation among nuclei and equals 3.61 for the Poissonian Voronoi network. Figure 3(a) shows the distribution of Voronoi cell areas fitted by the scaling function for each deposition amount. With increase in the surface coverage the scaled area distributions become narrower, thereby reflecting the increase of the coefficient α in Fig. 3(b). This implies the possibility for the kinetic self-ordering of 3D islands.^{23,24} Remarkably, this tendency continues even at the steady-state regime after deposition of 1.0 ML. The average area of the Voronoi cells then reaches about $1.4 \times 10^4 \text{ nm}^2$ in accordance with the intuition that the half distance between 3D islands should be on the order of the diffusion length $\sim 70 \text{ nm}$ on the wetting layer. Recently, Pimpinelli and Einstein²⁵ showed that an excellent description of the capture zone size distribution can be obtained by the generalized Wigner distribution (GWD),

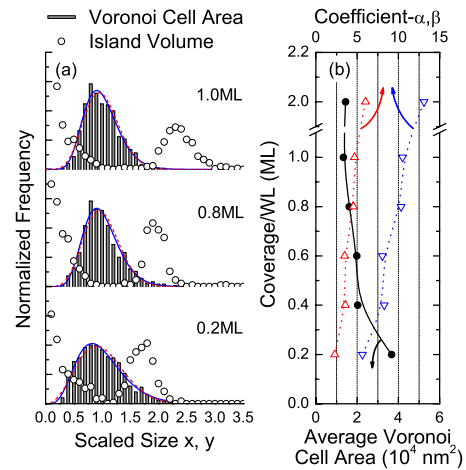


FIG. 3. (Color online) (a) Scaled distributions of Voronoi cell areas (vertical bars) fitted to two different scaling functions of the SGD (solid curves) and the GWD (short-broken curves), and scaled distributions of the experimental island size (open circles) in the submonolayer deposition range of 0.2, 0.8, and 1.0 ML on the wetting layer. x is the Voronoi cell area scaled with its average area, and y is the island volume scaled with its mean value. (b) Average area of the Voronoi cells (solid circles) and both coefficients of α (open downward triangles) and β (open upward triangles) as a function of Ge amount deposited on the wetting layer.

$$P_{\beta}(x) = a_{\beta} x^{\beta} \exp(-b_{\beta} x^2), \quad (2)$$

where the coefficient β is a parameter directly related to the critical nucleus size i with $\beta=i+1$. a_{β} and b_{β} are β -dependent constants determined by the normalization and the unit mean, respectively.²⁶ The nuclei that are composed of more than $i+1$ atoms grow to be further stable, but those with less than i atoms tend to decompose. The distribution of the scaled Voronoi cell area can be also fitted by the universal scaling function $P_{\beta}(x)$ [Fig. 3(a)]. The value of $\beta=4.68$ yields the critical nucleus size $i \sim 4$ for the deposition of 1.0 ML where the Voronoi cells coincide with the diffusion cells [Fig. 3(b)]. The obtained value of i may appear quite small when compared to the subcritical nucleus of several hundred atoms temporarily formed on the wetting layer at much lower temperature $T=300 \text{ }^{\circ}\text{C}$.²⁷ In general, the higher growth temperature would require larger critical nuclei to trigger the nucleation since adatom detachment from a nucleus edge cannot be negligible. However, the mass transport from the SiGe alloy wetting layer in the present study is so significant that not only Ge atoms but also Si atoms can be contained in the critical nucleus. The stronger bonding force of Si compared to that of Ge stabilizes the nucleus to reduce the critical nucleus size.²⁸ In the same line, the critical nucleus size of only $i=9$ has been reported for the growth of Ge/Si(111).²⁹

On the other hand, according to the capture zone model, also the distribution of the island volumes scaled with their mean volume is expected to follow a scaling function $f_i(y)$ such as the SGD and the GWD,^{25,30}

$$N_s(\Theta) = \frac{\Theta}{\langle s \rangle^2} f_i \left(\frac{s}{\langle s \rangle} \right), \quad (3)$$

where $N_s(\Theta)$ is the number of islands (normalized by the number of lattice sites) which is composed of s atoms. $\langle s \rangle$ is the average number of atoms contained in islands. This scale invariance also makes it possible to determine the critical nucleus size i . The statistical procedure was employed to describe the 2D homoepitaxial growth of Fe/Fe(001) (Refs. 30 and 31) and the 3D SK growth of InAs on GaAs(001).^{10,32–34} In the latter case, the surface coverage of $\Theta = \sum_s N_s$ is replaced by the effective thickness on the wetting layer, which is calculated from the total volume of 3D islands normalized to the area probed by AFM. Figure 3(a) shows the scaled distributions of the island size in the submonolayer deposition range of 0.2–1.0 ML on the 2D layer. Notice that none of the scaling functions above can represent the experimental data of bimodal distributions. The fact that the scaled size distributions have nonzero values around $y = 0$ resembles the characteristic observed in the distribution corresponding to the critical nucleus size $i = 0$.^{30,35} The nucleus having the zero critical size implies that the nuclei can exist inherently as single adatom on the wetting layer surface. The defects present at the wetting layer surface mediate nucleation without critical size. For instance, step edges and/or kinks are possible candidates for the nucleation sites. The growth of nucleus is encouraged by the substantial adatoms detached from the step edges of wetting layer. Such anomalous scaling behaviors supported by the observation of the nucleation at the step edges have been reported for the InAs islands on GaAs.¹⁰ In particular, the bimodal distribution can be reproduced by the model accounting for both preferential nucleation sites and significant exchange processes between deposited adatoms and the substrate atoms in the top surface.³⁶ These thermally activated exchange processes induce the incorporation of Si atoms into the nuclei at high temperature.

It is conceivable that the atomic interaction with the intermixed wetting layer occurs from the nucleation regime which can affect both the composition and strain in the growing islands. Here, Raman scattering spectroscopy was employed to probe the composition and strain states during the growth of Ge/Si nanoislands. Figure 4 shows Raman spectra obtained at different deposition amount of ^{76}Ge isotopes. The Raman spectrum of the wetting layer shows spectral features at ~ 225 , ~ 302 , and $\sim 435 \text{ cm}^{-1}$ corresponding to 2TA(L), 2TA(X), and 2TA(Σ) phonons of the Si substrate, respectively. No clear Raman feature due to the 4.4 ML 2D layer has appeared in accordance with the previous reports.^{37,38} Three peaks are observed at ~ 290 , ~ 408 , and $\sim 520 \text{ cm}^{-1}$, which are assigned to $^{76}\text{Ge}-^{76}\text{Ge}$, Si- ^{76}Ge , and Si-Si modes, respectively. As the nucleation and island growth proceeds on the wetting layer, the Raman signals of the $^{76}\text{Ge}-^{76}\text{Ge}$ and Si- ^{76}Ge modes become more pronounced. Note that the $^{76}\text{Ge}-^{76}\text{Ge}$ peak is separately observed on the lower-frequency shoulder of the substrate 2TA(X) peak due to the isotope effect.³⁹ The Ge-Ge mode arising from Ge having natural isotopic abundance would have overlapped completely with the substrate 2TA(X) peak. Hence, the use of

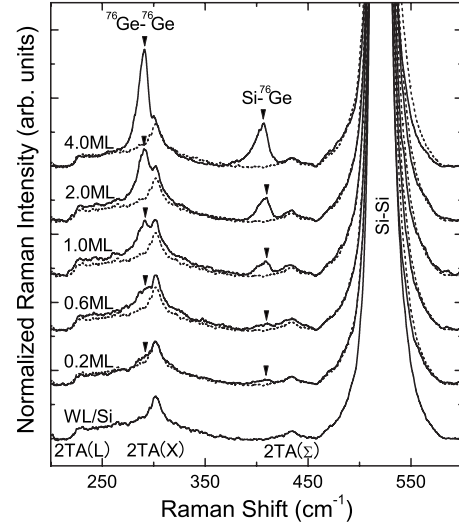


FIG. 4. Raman spectra obtained for different ^{76}Ge deposition amounts on the wetting layer. All spectra are normalized to the Si-Si mode of the substrate. For comparison, Raman spectrum of the wetting layer having the critical thickness (the bottom spectrum) is overlapped as the dotted curves with each spectrum.

enriched ^{76}Ge isotope source enables us to probe the faint signals of the small-sized 3D islands formed by submonolayer deposition. Figures 2(c)–2(e) show the average SiGe composition and compressive biaxial strain inside 3D islands that are determined from the peak positions of the $^{76}\text{Ge}-^{76}\text{Ge}$ and Si- ^{76}Ge modes.¹⁶ $b_{\text{Ge-Ge}} = -400 \text{ cm}^{-1}$ and $b_{\text{Si-Ge}} = -575 \text{ cm}^{-1}$ are used as the strain-shift coefficients,³⁷ and the isotopic shift due to ^{76}Ge is taken into account. Figures 2(c) and 2(d) also display the absolute amounts of Si and Ge atoms in the 3D islands estimated from the effective thickness on the wetting layer. Remarkably, the amounts of both Si and Ge atoms incorporated into 3D islands surpass the number of the evaporated Ge atoms on the wetting layer for the deposition of 0.2 ML, indicating that most of the atoms in nuclei are supplied from the SiGe alloy wetting layer at the nucleation regime. This implies that the initial strained SiGe alloy wetting layer is largely decomposed and incorporated into the more relaxed 3D islands when the deposition reaches 2.0 ML. Such a strong interaction with the metastable 2D layer has been observed also during formation of hut clusters at relatively low temperature.⁴⁰ Above 2.0 ML, the incorporation rate of Ge atoms approaches asymptotically the Ge deposition rate. This suggests that most of Ge adatoms deposited within the diffusion cells contribute to the growth of 3D islands. In parallel, Si atoms are further incorporated from the exposed silicon substrate.

The compressive strain inside the 3D islands relaxes as a general trend beyond the deposition amount of 1.0 ML [Fig. 2(e)]. It is well known that a large fraction of pyramids appears to undergo the pyramid-to-dome shape transition as a path for the partial relaxation of strain while some of the relatively strained pyramids decay.¹⁴ Note that the pyramid-derived plots in Fig. 1 progressively approach zero. The atoms released from the decaying pyramids contribute to the further growth of the adjacent relaxed domes as observed in the growth of InAs on GaAs(001).⁴¹ The driving force for the

island-island interaction is known to be the strain fields present around 3D islands.²³ When the 3D islands get close to each other, the interference of the strain fields induces a biased surface diffusion.⁴² Hence, the newly deposited Ge adatoms are not necessarily incorporated into the nearest neighboring islands. The effective capture zones around strained pyramids shrink whereas those around the neighboring relaxed domes expand. Therefore the simple capture zone model assuming a correlation coefficient of unity does not hold at the steady-state regime [Fig. 2(a)]. Furthermore, the coefficient α maintains a steady increase all the way up to the deposition of 2.0 ML [Fig. 3(b)] while the correlation coefficient r decreases after 1.0 ML [Fig. 2(a)]. The continuous lateral ordering can occur in conjunction with the strain-driven repulsive motions of closely spaced 3D islands.^{43,44}

IV. CONCLUSIONS

The nucleation and growth of Ge/Si(001) SK nanoisland have been investigated at temperature of $T=620$ °C. The correlation between the grown island volumes and the corresponding Voronoi cell areas shows clearly that the growth of the 3D islands does not follow the simple capture zone model. In addition to the deposited Ge adatoms, the material transferred from the alloyed 2D layer and underlying substrate contributes also to the growth of the strained islands. The atomic number of critical nucleus size is obtained from the scaling analysis of the distribution of the Voronoi cell areas. The experimental values of i , much smaller than anticipated, suggest that the simultaneous incorporation of Si atoms have a thermally stabilizing effect on the nuclei. The

strong interaction with the metastable 2D layer was found to occur from the nucleation regime. This is supported by the composition within the islands formed at the early stage of the growth process, which was determined from Raman analysis combined with ⁷⁶Ge isotope tracing. As soon as the 2D layer reaches the critical thickness, the formation of the nuclei is accelerated by the erosion of the intermixed 2D layer. When the surface is fully covered by the diffusion cells at the steady-state regime, most of the adatoms contribute to the growth of the existing 3D islands and no more nucleation takes place. The decrease in the distance between the neighboring islands promotes the strain-driven atomic transport especially between the strained pyramids and the adjacent relaxed domes. At the same time, the deposited Ge adatoms are not necessarily incorporated into the nearest neighboring islands. The island-island interaction unevenly deforms the capture zones around the islands of different sizes, leading to further lateral ordering.

ACKNOWLEDGMENTS

The authors acknowledge B. Voigtländer and Y. Saito for valuable discussions and O. D. Dubon for Rutherford back-scattering spectroscopy measurements. O.M. is grateful to the Japan Society for Promotion of Science for the financial support. This work was supported in part by Grant-in-Aid for Scientific Research by MEXT (Specially Promoted Research No. 18001002) in part by Special Coordination Funds for Promoting Science and Technology and in part by Grant-in-Aid for the Global Center of Excellence for High-Level Global Cooperation for Leading-Edge Platform on Access Spaces from MEXT.

*satoru@appi.keio.ac.jp

†moutanab@mpi-halle.mpg.de

‡kitoh@appi.keio.ac.jp

¹J. Stangl, V. Holý, and G. Bauer, *Rev. Mod. Phys.* **76**, 725 (2004).

²I. N. Stranski and L. Krastanow, *Sitzungsber. Akad. Wiss. Wien, Math.-Naturwiss. Kl., Abt. 2B* **146**, 797 (1938).

³M. Kästner and B. Voigtländer, *Phys. Rev. Lett.* **82**, 2745 (1999).

⁴R. E. Rudd, G. A. D. Briggs, A. P. Sutton, G. Medeiros-Ribeiro, and R. S. Williams, *Phys. Rev. Lett.* **90**, 146101 (2003).

⁵K. Shibata and K. Hirakawa, *Appl. Phys. Lett.* **93**, 062101 (2008); M. Jung, T. Machida, K. Hirakawa, S. Komiyama, T. Nakaoka, S. Ishida, and Y. Arakawa, *ibid.* **87**, 203109 (2005).

⁶K. Nakajima, A. Konishi, and K. Kimura, *Phys. Rev. Lett.* **83**, 1802 (1999).

⁷X. R. Qin, B. S. Swartzentruber, and M. G. Lagally, *Phys. Rev. Lett.* **84**, 4645 (2000).

⁸P. A. Mulheran and J. A. Blackman, *Phys. Rev. B* **53**, 10261 (1996).

⁹F. Ratto, A. Locatelli, S. Fontana, S. Kharrazi, S. Ashtaputre, S. K. Kulkarni, S. Heun, and F. Rosei, *Phys. Rev. Lett.* **96**, 096103 (2006); F. Ratto, Ph.D. thesis, Université du Québec, 2007.

¹⁰M. Fanfoni, E. Placidi, F. Arciprete, E. Orsini, F. Patella, and A.

Balzarotti, *Phys. Rev. B* **75**, 245312 (2007); F. Arciprete, E. Placidi, V. Sessi, M. Fanfoni, F. Patella, and A. Balzarotti, *Appl. Phys. Lett.* **89**, 041904 (2006); E. Placidi, F. Arciprete, V. Sessi, M. Fanfoni, F. Patella, and A. Balzarotti, *ibid.* **86**, 241913 (2005).

¹¹B. Voigtländer, *Surf. Sci. Rep.* **43**, 127 (2001).

¹²G. Katsaros, G. Costantini, M. Stoffel, R. Esteban, A. M. Bittner, A. Rastelli, U. Denker, O. G. Schmidt, and K. Kern, *Phys. Rev. B* **72**, 195320 (2005).

¹³T. U. Schüllli, M.-I. Richard, G. Renaud, V. Favre-Nicolin, E. Wintersberger, and G. Bauer, *Appl. Phys. Lett.* **89**, 143114 (2006).

¹⁴F. M. Ross, J. Tersoff, and R. M. Tromp, *Phys. Rev. Lett.* **80**, 984 (1998).

¹⁵A. Rastelli, M. Stoffel, J. Tersoff, G. S. Kar, and O. G. Schmidt, *Phys. Rev. Lett.* **95**, 026103 (2005).

¹⁶M. I. Alonso, M. de la Calle, J. O. Ossó, M. Garriga, and A. R. Goñi, *J. Appl. Phys.* **98**, 033530 (2005).

¹⁷A. V. Baranov, A. V. Fedorov, T. S. Perova, R. A. Moore, V. Yam, D. Bouchier, V. Le Thanh, and K. Berwick, *Phys. Rev. B* **73**, 075322 (2006).

¹⁸A. Malachias, S. Kycia, G. Medeiros-Ribeiro, R. Magalhães-Paniago, T. I. Kamins, and R. S. Williams, *Phys. Rev. Lett.* **91**, 176101 (2003).

- ¹⁹T. U. Schüllli, M. Stoffel, A. Hesse, J. Stangl, R. T. Lechner, E. Wintersberger, M. Sztucki, T. H. Metzger, O. G. Schmidt, and G. Bauer, *Phys. Rev. B* **71**, 035326 (2005).
- ²⁰A. Ishizaka and Y. Shiraki, *J. Electrochem. Soc.* **133**, 666 (1986).
- ²¹M. Li, M. C. Bartelt, and J. W. Evans, *Phys. Rev. B* **68**, 121401(R) (2003).
- ²²U. Denker, O. G. Schmidt, N. Y. Jin-Phillipp, and K. Eberl, *Appl. Phys. Lett.* **78**, 3723 (2001).
- ²³M. Meixner, E. Schöll, V. A. Shchukin, and D. Bimberg, *Phys. Rev. Lett.* **87**, 236101 (2001); M. Meixner, E. Schöll, M. Schmidbauer, H. Raidt, and R. Köhler, *Phys. Rev. B* **64**, 245307 (2001).
- ²⁴B. Cho, T. Schwarz-Selinger, K. Ohmori, D. G. Cahill, and J. E. Greene, *Phys. Rev. B* **66**, 195407 (2002).
- ²⁵A. Pimpinelli and T. L. Einstein, *Phys. Rev. Lett.* **99**, 226102 (2007); B. R. Conrad, E. Gomar-Nadal, W. G. Cullen, A. Pimpinelli, T. L. Einstein, and E. D. Williams, *Phys. Rev. B* **77**, 205328 (2008).
- ²⁶ $a_\beta = 2\Gamma(\frac{\beta+2}{2})^{\beta+1} / \Gamma(\frac{\beta+1}{2})^{\beta+2}$ and $b_\beta = [\Gamma(\frac{\beta+2}{2}) / \Gamma(\frac{\beta+1}{2})]^2$.
- ²⁷D. E. Jesson, M. Kästner, and B. Voigtländer, *Phys. Rev. Lett.* **84**, 330 (2000).
- ²⁸V. Cherepanov and B. Voigtländer, *Phys. Rev. B* **69**, 125331 (2004).
- ²⁹A. A. Shklyaev, M. Shibata, and M. Ichikawa, *Surf. Sci.* **416**, 192 (1998).
- ³⁰J. G. Amar and F. Family, *Phys. Rev. Lett.* **74**, 2066 (1995).
- ³¹J. A. Strosio and D. T. Pierce, *Phys. Rev. B* **49**, 8522(R) (1994).
- ³²V. Bressler-Hill, S. Varma, A. Lorke, B. Z. Nosho, P. M. Petroff, and W. H. Weinberg, *Phys. Rev. Lett.* **74**, 3209 (1995).
- ³³Y. Ebiko, S. Muto, D. Suzuki, S. Itoh, K. Shiramine, T. Haga, Y. Nakata, and N. Yokoyama, *Phys. Rev. Lett.* **80**, 2650 (1998).
- ³⁴T. J. Krzyzewski, P. B. Joyce, G. R. Bell, and T. S. Jones, *Phys. Rev. B* **66**, 201302(R) (2002).
- ³⁵D. D. Chambliss and K. E. Johnson, *Phys. Rev. B* **50**, 5012(R) (1994).
- ³⁶R. Miranda and J. M. Gallego, *Phys. Rev. B* **64**, 085426 (2001).
- ³⁷P. H. Tan, K. Brunner, D. Bougeard, and G. Abstreiter, *Phys. Rev. B* **68**, 125302 (2003).
- ³⁸O. Moutanabbir, S. Miyamoto, A. Fujimoto, and K. M. Itoh, *J. Cryst. Growth* **301-302**, 324 (2007).
- ³⁹A. V. Kolobov, K. Morita, K. M. Itoh, and E. E. Haller, *Appl. Phys. Lett.* **81**, 3855 (2002).
- ⁴⁰M. Horn-von Hoegen, B. H. Müller, T. Grabosch, and P. Kury, *Phys. Rev. B* **70**, 235313 (2004).
- ⁴¹T. R. Ramachandran, R. Heitz, P. Chen, and A. Madhukar, *Appl. Phys. Lett.* **70**, 640 (1997).
- ⁴²M. Stoffel, A. Rastelli, S. Kiravittaya, and O. G. Schmidt, *Phys. Rev. B* **72**, 205411 (2005).
- ⁴³U. Denker, A. Rastelli, M. Stoffel, J. Tersoff, G. Katsaros, G. Costantini, K. Kern, N. Y. Jin-Phillipp, D. E. Jesson, and O. G. Schmidt, *Phys. Rev. Lett.* **94**, 216103 (2005).
- ⁴⁴G. Capellini, M. De Seta, F. Evangelisti, V. A. Zinovyev, G. Vastola, F. Montalenti, and Leo Miglio, *Phys. Rev. Lett.* **96**, 106102 (2006).